Influence of Spin-Dependent Level Densities and Gamma-Ray Competition in the Decay of Highly Excited Nuclei*

MARSHALL BLANN
Nuclear Structure Research Laboratory
and
Department of Chemistry, University of Rochester, Rochester, New York
(Received 15 September 1966; revised manuscript received 16 February 1967)

Excitation functions for the $Fe^{56}(\alpha,pxn)$ reactions ($x=1$ to 4) have been calculated with the statistical theory of nuclear reactions, using optical-model transmission coefficients for neutrons, protons, and α particles and a level density of the form $\rho(E,J) \propto (2J+1)\rho(E-E_{\mathrm{rot}})$, where $E_{\mathrm{rot}}=J(J+1)\hbar^2/2\vartheta_{\mathrm{rig}}R$. Here ϑ_{rig} is the rigid-body moment of inertia, and the dimensionless parameter R was taken in different calculations as 1 or ∞. Where a rigid body moment of inertia was used, two assumptions were made concerning γ-ray de-excitation: It was assumed that (a) there was no γ-ray competition if the excitation energy exceeded the minimum nucleon binding energy, or (b) there was no γ-ray competition if the excitation exceeded the binding energy plus rotational energy for each spin. Of the three sets of calculations, the latter set gave the best over-all agreement with experimental (α,pn) and $(\alpha,p2n)$ excitation functions. Calculations were also performed for the $Ti^{48}(C^{12},pxn)$ excitation functions (where $Ti^{48}+C^{12}$ forms the same compound nucleus as $Fe^{56}+\alpha$), where $x=1$ to 4, with $R=1.0$, and assumption (b) concerning γ-ray–nucleon emission competition. It is concluded that excitation-function measurements to test the influence of angular momentum on the independence hypothesis should show observable differences in shape and energy dependence, but that a good knowledge of E and dE/dX for the heavy ion is required if one is to be confident of the interpretation of the results. The influence of γ-ray competition based on assumption (b) is considered as a function of mass number of the compound nucleus; the qualitative differences expected for actual excitation functions with respect to the predictions of the Weisskopf-Ewing evaporation model with no γ-ray competition should decrease with an increase in mass number. Specifically, excitation functions from lower-mass compound nuclei should be broader, should be displaced to higher energies, and should have more pronounced high-energy tails than those from heavier-mass systems.

I. INTRODUCTION

MUCH recent interest has centered on the role of angular momentum in the decay of highly excited nuclei with relatively high angular momenta.[1–7] Questions have been raised on the importance and degree of gamma-ray competition with particle emission in the final stages of the evaporation cascades, and of the importance of angular-momentum conservation restrictions on decay-rate calculations in which a finite rather than an infinite moment of inertia is assumed.

Several types of experimental measurements have been performed relevant to these questions, primarily isomer-ratio studies,[8,9] and experiments of the type performed by Ghoshal in which a compound nucleus is formed with different projectile-target combinations, so that at a given excitation energy the compound nuclei have different spin distributions.[10–12] Comparison of sets of excitation functions or particle spectra should then provide qualitative information on the role of angular momentum in these reactions. A more quantitative appreciation of the reaction would result from a comparison of a detailed set of calculated values with those measured experimentally, the agreement being checked for various inputs to the calculations. The mathematical intractability of the statistical theory has tended to prevent such comparison; generally, assumptions of some sort are made prior to applying the statistical theory, and it is often the case that a rigorous calculation would be required to assess the validity of these approximations.

Recently, calculations have been performed in which the common approximation of an infinite moment of inertia was not made for systems where several particles may be emitted[13,14]; it is the purpose of this work to present results of one such set of calculations. The compound nucleus Ni^{60} is assumed to be produced by $Fe^{56}+\alpha$ and $Ti^{48}+C^{12}$ bombardment yielding compound nuclei at excitations of 18–70 MeV; we then investigate the predicted excitation functions resulting from the decay of these nuclei for the assumptions that the nuclear moment of inertia has the rigid-body value, and that it is infinite. For the former assumption, we investigate two relatively opposite and extreme assump-

* This work was primarily supported by the U. S. Atomic Energy Commission.
[1] D. Sperber, Phys. Rev. **142**, 478 (1966).
[2] D. Sperber, Phys. Rev. **138**, B1024 (1965); **138**, B1028 (1965).
[3] D. Sperber, Nuovo Cimento **36**, 1164 (1965).
[4] J. R. Grover, Phys. Rev. **127**, 2142 (1962).
[5] J. R. Grover, Phys. Rev. **123**, 267 (1961).
[6] T. D. Thomas, Nucl. Phys. **53**, 558, 577 (1964).
[7] J. O. Rasmussen and T. T. Sugihara, Phys. Rev. **151**, 992 (1966).
[8] T. Matsuo, J. M. Matuszek, Jr., N. D. Dudey, and T. T. Sugihara, Phys. Rev. **139**, B886 (1965); **139**, B896 (1965).
[9] D. G. Sarantites, Nucl. Phys. **A93**, 576 (1967).
[10] S. N. Ghoshal, Phys. Rev **80**, 939 (1950).
[11] C. M. Stearns and J. M. Miller (to be published).
[12] G. Simonoff and J. M. Alexander, in *Proceedings of the Third Conference on Reactions Between Complex Nuclei*, edited by A. Ghiorso, R. M. Diamond, and H. E. Conzett (University of California Press, Berkeley, 1963), p. 345.
[13] J. R. Grover and J. Gilat, this issue, Phys. Rev. **157**, 802 (1967); **157**, 814 (1967); **157**, 823 (1967).
[14] D. G. Sarantites and B. D. Pate, Nucl. Phys. **A93**, 545 (1967).

tions concerning the competition of γ rays with particle emission. Calculated $Fe^{56}(\alpha,pxn)$ excitation functions ($x=1, 2, 3, 4$) are compared with experimentally measured values[15] to gain insight into the validity of the statistical theory itself, and the importance of assumptions concerning moments of inertia and γ-ray competition in the decay of these compound nuclei. The importance and qualitative behavior of these effects as a function of mass number is discussed as well.

II. CALCULATION

In this section we first define symbols and present the rate equations to be used in the calculations of this work. We next define the functional form selected for the spin-dependent level density, and discuss the parameters selected for both the level-density expression and transmission coefficients. We discuss next the program logic and debugging procedures, and finally the assumptions which have been made for γ-ray competition with particle emission, and the reasons for making these assumptions. The calculations were performed on a CDC-6600 computer, for compound nuclei at 21 initial excitations between 17 and 70 MeV.

For the calculations to be discussed, emission of neutrons, protons, and α particles has been considered; the particle type will be denoted by either a subscript or superscript ν. At any stage of a cascade the angular momentum of the emitting nuclide will be denoted by I, that of the product nuclide by J. The intrinsic particle spin of particle ν is denoted by s_ν, channel spin by S (where $S=\mathbf{J}+\mathbf{s}$), transmission coefficients for capture of a particle ν with orbital angular momentum l, and channel energy ϵ by $T_l{}^\nu(\epsilon)$. Energies of excitation of product nuclides will be denoted by E, those of emitting nuclides by E^*.

The rate for emitting a particle ν from a compound nucleus with spin I and excitation E^* to form a residual nucleus with angular momentum J and excitation E has been given as[6]

$$R(E,J)dE \propto \frac{\rho(E,J)}{\rho(E^*,I)} \sum_{S=|J-s_\nu|}^{J+s_\nu} \sum_{l=|I-S|}^{I+S} T_l{}^\nu(\epsilon)d\epsilon. \quad (1)$$

By assuming that for spin-zero or spin-$\frac{1}{2}$ particles, as are considered in this work, that the sum over S may be replaced by a factor $2s_\nu+1$, by rearranging the order of summation, and by normalizing over emission of all possible particles and energies, one obtains an expression for the probability per unit time of emitting a particle ν with channel energy between ϵ and $\epsilon+d\epsilon$ from an emitting nucleus of spin I,

$$P_\nu(\epsilon,I)d\epsilon = (2s_\nu+1)\sum_{l=0}^{\infty} T_l{}^\nu(\epsilon) \sum_{J=|I-l|}^{I+l} \rho(E,J)d\epsilon \Big/ \left[\int_{\epsilon=0}^{\infty} \sum_{\nu=1}^{n} (2s_\nu+1)\sum_{l=0}^{\infty} T_l{}^\nu(\epsilon) \sum_{J=|I-l|}^{I+l} \rho(E,J)d\epsilon\right], \quad (2)$$

and the cross section $\sigma_\nu(\epsilon)$ is given by

$$\sigma_\nu(\epsilon)d\epsilon = \pi\lambda\!\!\!^{-2} \sum_{I=0}^{\infty} (2I+1)T_I P_\nu(\epsilon,I)d\epsilon, \quad (3)$$

where T_I is the transmission coefficient for formation of the compound nucleus with the Ith partial wave of the incident particle, and $\lambda\!\!\!^{-}$ is the reduced de Broglie wavelength of the bombarding particle. As I and T_I are defined, it is obvious that we have assumed zero ground-state spin for target nuclei; Vonach and Huizenga have shown in a rigorous calculation involving Co^{59} (spin $\frac{7}{2}$) that this approximation produces no significant error.[16]

A. Level-Density Expression

Several forms have been presented for spin-dependent level densities,[17,18] i.e.,

$$\rho(E,J) \propto (2J+1)\rho(E)\exp[-J(J+1)\hbar^2/2\sigma^2], \quad (4)$$

where σ^2 is the so-called spin-cutoff parameter, and

$$\rho(E,J) \propto (2J+1)\rho\left(E-\frac{J(J+1)\hbar^2}{2\mathcal{I}}\right) = (2J+1)\rho(E'), \quad (5)$$

where $\mathcal{I}$ represents the nuclear moment of inertia. In Eq. (5), the angular momentum is treated purely as a classical rotational energy $E_{\rm rot}$, so that the thermodynamic excitation E is replaced by $E-E_{\rm rot}=E'$.

Equation (4) has the undesirable feature of predicting arbitrarily high spin levels at any excitation, a situation which is not physically realistic for a system composed of a finite number of nucleons. One would expect that, for a specific angular momentum J, there would be some minimum value of E below which no levels of spin J may be populated.[17] We shall refer to this energy as E_c, the subscript denoting that this is the energy at the cutoff point. The level density given by Eq. (5) has the advantage of a smooth decrease with increasing spin in the region of the cutoff until a point is reached at which the rotational energy equals the thermodynamic excitation energy; beyond this point the level density has been assumed to be zero. We therefore assume, on the basis of results by Sperber,[1] that

$$E_c = E_{\rm rot} = \frac{J(J+1)\hbar^2}{2\mathcal{I}}. \quad (6)$$

[15] A. Ewart, C. Valentine, and M. Blann, Nucl. Phys. **69**, 625 (1965).

[16] H. K. Vonach and J. R. Huizenga, Phys. Rev. **149**, 844 (1966).

[17] T. Ericson, Advan. Phys. **9**, 425 (1960).

[18] D. W. Lang, Nucl. Phys. **77**, 545 (1966).

The level density of Eq. (5) may be rewritten with the rotational energy term as

$$E_{\rm rot}=\frac{J(J+1)\hbar^2}{2\mathcal{I}_{\rm rig}R}, \tag{7}$$

where $\mathcal{I}_{\rm rig}$ represents the rigid-body moment of inertia, and the parameter $R=\mathcal{I}/\mathcal{I}_{\rm rig}$, the ratio of assumed moment of inertia to rigid-body value. In this way R becomes a convenient input parameter for the computer program. In this work calculations have been done with $R=1.0$ and $R=\infty$ (actually 10^4 was used). In the latter case, Eq. (2) reduces to the Weisskopf-Ewing evaporation formula[19]

$$P_\nu(\epsilon)d\epsilon=\frac{(2s_\nu+1)\mu_\nu\epsilon_\nu\sigma_\nu(\epsilon)\rho(E)d\epsilon}{\int_{\epsilon=0}^{\infty}\sum_{\nu=1}^{n}(2s_\nu+1)\mu_\nu\epsilon_\nu\sigma_\nu(\epsilon)\rho(E)d\epsilon}, \tag{8}$$

where μ_ν is the reduced mass of the particle ν, $\sigma_\nu(\epsilon)$ is the inverse reaction cross section, and $\rho(E)$ is the total level density of the residual nucleus at excitation energy E. We have made use of this equivalence in program debugging, as will be described in Sec. II D.

The level density of Eq. (5) was taken to be of the functional form[17]

$$\rho(E')\propto\frac{1}{(E'-\delta)^2}\exp\{2[a(E'-\delta)]^{1/2}\}, \tag{9}$$

where δ is a condensation (pairing) energy to correct for odd-even effects.

B. Parameter Evaluation

1. Level-Density Parameters

(*a*) *Level-Spacing Parameter.* The level-spacing parameter a of Eq. (9) was assumed to be 7.0 MeV^{-1}, in agreement with values derived from particle spectral measurements from $Co^{59}(p,\alpha)$ and $Fe^{56}(\alpha,\alpha')$ reactions.[20,21] The experimental α-particle spectra were analyzed with a level density expression similar to that of Eq. (9).

(*b*) *Pairing Energy.* The pairing energy δ of Eq. (9) was evaluated from the mass tabulation of Everling *et al.*[22] as half the difference between even-A nuclidic-mass excess versus Z parabolas. A value of $\delta=0$ MeV was used for odd-odd nuclides, 1.4 MeV for odd-mass nuclides, and 2.8 MeV for even-even nuclides. The reasons for using such condensation energies in computing level densities has been discussed by other authors.[23]

(*c*) *Nuclear Moment of Inertia.* The rigid-body moment of inertia $\mathcal{I}_{\rm rig}=\frac{2}{5}MR^2$ was calculated with $r_0=1.2A^{1/3}$ F; this value was based on a spin-cutoff analysis of the anisotropy of the $Fe^{56}(\alpha,\alpha')$ reaction by Benveniste *et al.*[21] As mentioned previously, R values of 1.0 and ∞ were used in Eq. (7). It is not the purpose of this work to find a "best value" for R by variation and comparison with experimental results. There is, in fact, no single best value to be found with the current state of theoretical understanding. Extraction of such a value would require a better knowledge of the nuclear level-density function near the cutoff region, a knowledge of absolute radiative-decay rates versus particle-emission rates, and a more complete knowledge of n, p, and α transmission coefficients for large l, corresponding classically to the region of the nuclear surface and beyond. Different assumptions for these values will lead to different values for the moment of inertia.[8] The approach of this work is, therefore, only to understand the types and magnitude of changes one observes for differing values of R; the two values selected should permit attainment of this goal.

2. Transmission Coefficients

The n and p transmission coefficients were taken from the compilations of Mani *et al.*,[24,25] and were used in the laboratory system, since the corrections to channel energies were quite small. A single set of values was used for neutrons, corresponding to $A=58$; different sets of proton and α transmission coefficients were used for each Z. The $T_l^\alpha(\epsilon)$ were taken from the compilation of Igo and Huizenga,[26] and were converted to appropriate channel energies by graphical interpolation and extrapolation. Transmission coefficients were used down to $T_l^\nu\geq10^{-5}$; values of zero were used below these limits. Values were used for channel energies of 1–35 MeV in 1-MeV increments. Partial waves up to $l=23\hbar$ were used for n, p, and α particles emitted in reactions. Initial spin populations for compound nuclei up to $I=42\hbar$ were used, with residual nuclide spins up to $80\hbar$ being permitted.

The populations for each partial wave for forming the compound nuclei were obtained from the optical-model program of Auerbach for C^{12}, and of Bjorklund and Fernbach for α particles.[27,28] The parameters used were those of Huizenga and Igo for α particles.[27] Calculations

[19] V. F. Weisskopf and D. H. Ewing, Phys. Rev. **57**, 472 (1940).
[20] R. Sherr and F. P. Brady, Phys. Rev. **124**, 1928 (1961).
[21] J. Benveniste, G. Merkel, and A. Mitchell, Phys. Rev. **141**, 980 (1966).
[22] F. Everling, L. A. Konig, J. H. E. Mattauch, and A. H. Wapstra, *1960 Nuclear Data Tables, Part I* (U. S. Government Printing Office, Washington, D. C., 1960); also Nucl. Phys. **18**, 529 (1960).
[23] H. Hurwitz and H. Bethe, Phys. Rev. **81**, 898 (1951).
[24] G. S. Mani, I. Iori, and M. A. Melkanoff, Centre D'Etudes Nucléaires de Saclay Rapport C.E.A. No. 2379, 1963 (unpublished).
[25] G. S. Mani, I. Iori, and M. A. Melkanoff, Centre D'Etudes Nucléaires de Saclay Rapport C.E.A. No. 2380, 1963 (unpublished).
[26] J. R. Huizenga and G. J. Igo, Argonne National Laboratory Report No. 6373, 1961 (unpublished). See also Nucl. Phys. **29**, 462 (1962).
[27] We thank Professor J. M. Miller for help in obtaining the results from the ABACUS program written by E. H. Auerbach.
[28] F. E. Bjorklund and S. Fernbach, in *Proceedings of the Second International Conference on the Peaceful Uses of Atomic Energy, Geneva, 1958* (United Nations, Geneva, 1958), Vol. 14, p. 24.

were not performed for compound nuclei formed with C^{12} energies of less than 16 MeV, since the Coulomb wave function in the optical-model program used may not give proper convergence in this region. While the total calculated cross sections were showing the expected exponential decrease with energy below the lowest values used in this work, this does not justify the assumption that the results are physically accurate in this region.

C. Program Logic

The computation of this work was done by pointwise evaluation rather than by a Monte Carlo method. Arrays dimensioned in residual energy E and spin J were set up for the cross section populating each mass A and atomic number Z of reaction products, i.e., $\sigma(Z,A,E,J)$. Equations (2) and (3) were then applied starting with the compound nucleus. The $\sigma(Z,A,E,J)$ populations were computed for products resulting from n, p, and α emission from the compound nucleus (Z,A) populating $\sigma(Z, A-1, E, J)$, $\sigma(Z-1, A-1, E, J)$, and $\sigma(Z-2, A-4, E, J)$; the kinetic energies for emitted particles started at 1 MeV and increased in 1-MeV increments; orbital angular momenta were varied from 0 to a maximum (determined by input parameters) for each channel energy. In addition to the $\sigma(Z,A,E,J)$ arrays, the respective n, p, and α kinetic energy spectra as a function of kinetic energy ϵ and orbital angular momentum l, $\sigma(\epsilon,l)$, were also included in the output.

After all particle emission from the compound nucleus (Z,A) had been calculated, the population of $\sigma(Z, A-1, E, J)$ was taken as the emitting system, and the calculation described above was repeated. This was continued until all possible emission from atomic number Z was completed with respect to available excitation energy. At this point, the population $\sigma(Z-1, A-1, E, J)$ became the population of the emitting nucleus and the evaporation cascade was again followed for decreasing mass numbers until there was no energy for further emission. This process was repeated until emission from all nuclides of interest had been computed.

D. Debugging

Initial program tests were performed using selected transmission coefficients of unity, with all others being zero. When slide-rule calculations indicated that all values computed were being stored properly, a more rigorous test was applied, as described in the following paragraph.

Decks of transmission coefficients for n, p, and α emission from Ni and Co nuclei were used as input for a program which computed inverse reaction cross sections, i.e.,

$$\sigma_\nu(\epsilon)=\pi\lambda\!\!\!^{-2}\sum_{l=0}^{\infty}(2l+1)T_l^\nu(\epsilon). \qquad (10)$$

The inverse reaction cross sections so generated were in turn used as input into a Weisskopf-Ewing evaporation calculation for Ni^{60} nuclei at 42-MeV of excitation using a program previously described.[29] The same calculation was run with the program described in the previous subsection, using an input parameter $R=\mathcal{I}/\mathcal{I}_{\rm rig}=10^4$, i.e., essentially an infinite moment of inertia. The Weisskopf-Ewing calculation took approximately 0.5 min on an IBM 7074, while the calculation using transmission coefficients took nearly 90 min. Initially a few errors were found which hand calculations had not shown to be present; these were corrected, after which kinetic energy spectra, residual excitations, and integrated cross sections for nine residual nuclides (covering several thousand differential values) agreed in all cases for the two calculations.

E. Gamma-Ray–Particle-Emission Competition

Considerable attention has been directed at the expected enhancement of γ-ray-emission competition versus particle emission toward the end of an evaporative emission cascade.[4,5,17] The qualitative arguments for such an effect are most easily described with respect to the contour diagrams, $\sigma(Z,A,E,J)$, of Fig. 1. The sloping curve with parallel lines (e.g., in the contour for the population of Ni^{58}) represents a rather arbitrary approximation of the region in which the level density is zero, as discussed in Sec. II A. It may be seen that there exists a populated region toward the higher spin values where there is sufficient energy for the emission of an additional nucleon, but where a vertical displacement by the nucleon binding energy would result in an attempt to populate the region of zero level density. In this situation the requirement for nucleon emission is one of very high orbital angular momentum, aligned strongly antiparallel with the total-angular-moment vector of the emitting nucleus. Classically this requirement of large l values corresponds to emission from distances far outside the nuclear surface. Since the transmission coefficients are approaching zero for these conditions, the probability of particle emission per unit time decreases sharply with increasing l, giving a relative enhancement to gamma-ray cascades (which may go into a region of nonzero level density since no binding-energy requirement is involved).

The most desirable approach to the problem of gamma-ray deexcitation would be an explicit inclusion in the calculations described in this section. Some of the difficulties in such an approach are (1) ignorance of relative rates of nucleon emission versus γ-ray emission in the region of interest, in particular for the very highly distorted, high-spin nuclei in question; (2) an uncertainty (by perhaps several orders of magnitude) as to the level density in the region of the spin cutoff, which in turn determines the probability of nucleon emission

[29] M. Blann, Nucl. Phys. **80**, 223 (1966).

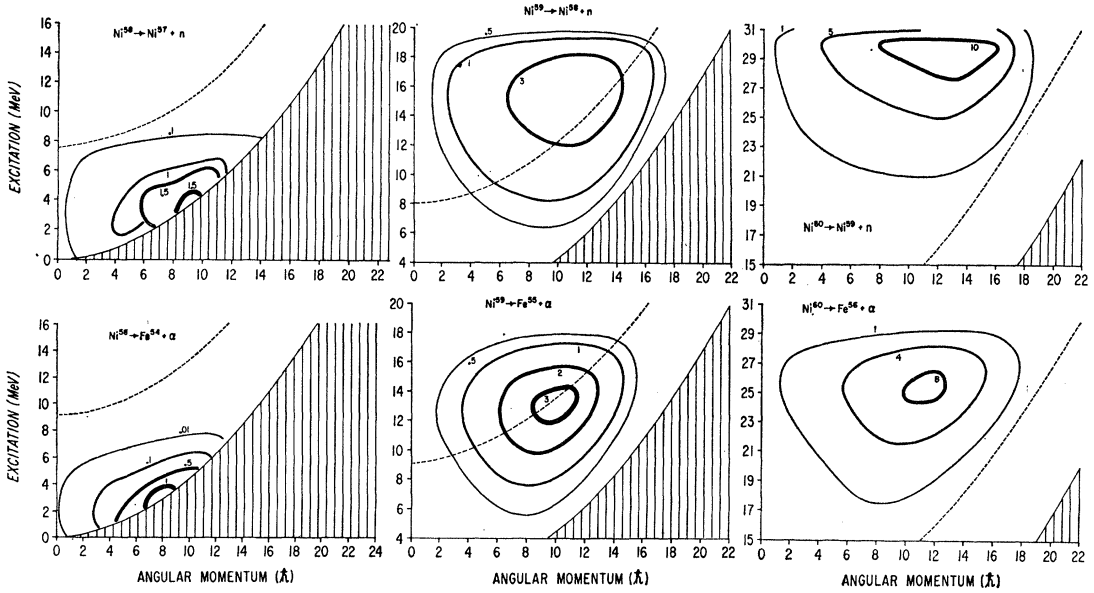

FIG. 1. Population contours of differential cross section as a function of residual excitation and angular momentum following emission of one, two, and three neutrons, and one alpha particle following emission of zero to two neutrons from a Ni^{60} nucleus at 40 MeV of excitation. The contour population numbers shown are in units of millibarns, with the contour curves smoothly connecting points calculated at unit energy and spin values. The results shown in this figure were calculated assuming a rigid-body moment of inertia. The parallel vertical lines indicate the spin-cutoff region where no levels are available because of angular-momentum restrictions. The dashed curve represents the binding energy of the least tightly bound nucleon above the spin-cutoff curve.

into this region; and (3) an uncertainty in transmission coefficients (again by several orders of magnitude) for nucleon emission far beyond the classical limits of the nuclear surface. In view of these difficulties, the approach adopted in this work is one of comparing the results of two relatively extreme and opposite assumptions concerning gamma-ray emission, to see qualitatively the influence of the effect described above. Comparisons between these calculated results and experimental measurements (in the following section) will

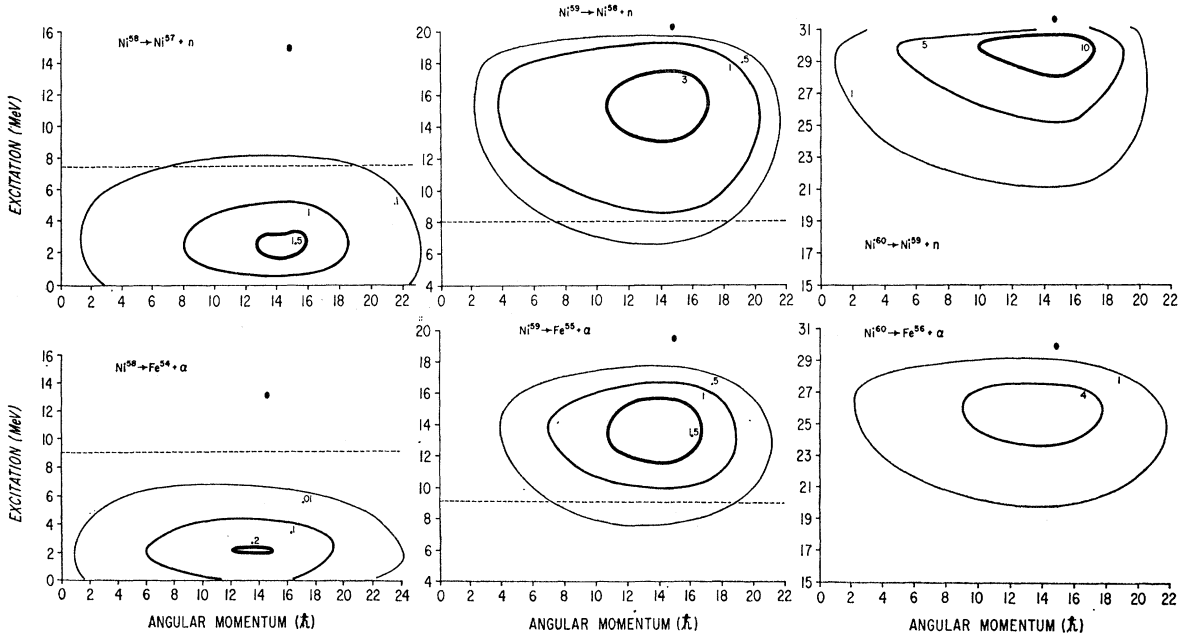

FIG. 2. This figure is similar to Fig. 1 except that an infinite moment of inertia was used in the calculation. The small circles represent the average spin of the initial compound nucleus; their position on the energy axis has no significance.

perhaps give some indication as to which assumption is nearer the truth from a quantitative standpoint.

The first assumption used in integrating (actually summing) the contours of Fig. 1 is that gamma-ray emission never competes where particle emission is energetically possible; thus the cross section for production of a given nuclide is the integral of the contour surface lying at excitations below the binding energy of the least tightly bound nucleon (e.g., if the horizontal dashed line in Fig. 2 were superimposed on Fig. 1), i.e.,

$$\Gamma_\gamma/\Gamma_T=0, \quad \text{if} \quad E>\text{BE}, \tag{11}$$

where E represents the excitation energy and BE the n or p binding energy, and Γ_γ and Γ_T represent the γ-ray and total decay widths, respectively. The same limit of integration was used in the calculations for which $R=10^4$ was assumed; some of these E-J contours are shown in Fig. 2.

A second set of integrations was performed with the assumption that particle emission does not compete with photon emission if the excitation is not sufficient to be above the parabolic cutoff determined by the rotational energy, i.e.,

$$\Gamma_\gamma/\Gamma_T=1 \text{ if } E(\text{MeV})<\text{BE}+J(J+1)\hbar^2/2\mathcal{I}_{\text{rig}}+1 \tag{12a}$$

and

$$\Gamma_\gamma/\Gamma_T=0 \text{ if } E(\text{MeV})\geq\text{BE}+J(J+1)\hbar^2/2\mathcal{I}_{\text{rig}}+1, \tag{12b}$$

where BE represents the binding energy of the least tightly bound nucleon, and 1 represents the minimum kinetic energy a nucleon must have for emission (due to the grid size used in these calculations). This limit of integration is represented in the contours of Fig. 1 as a dashed curve displaced above the solid rotational energy cutoff curve by the binding energy of the least tightly bound nucleon. It should be emphasized that the limits described by Eqs. (12a) and (12b) are arbitrary, and may or may not represent an upper limit to the γ-ray competition with particle emission.

III. RESULTS AND DISCUSSION

The results of calculations to be presented in this section may be divided into three parts. First, we shall present calculated excitation functions for the Fe^{56}-(α,pxn) reactions with two different assumptions of γ-ray versus particle-emission competition ($R=1.0$) as well as results for the same reactions with $R=\infty$. We will discuss the differences between the three sets of calculated excitation functions, and compare them with measured values. Second, a type of experiment intended to show angular-momentum effects will be considered, specifically a comparison between the excitation functions calculated for the systems $Ti^{48}(C^{12},pxn)Co^{59-x}$ and $Fe^{56}(\alpha,pxn)Co^{59-x}$, where $x=1$ to 4. From these comparisons we show the type and magnitude of deviations which might be expected between corresponding reactions when R is not infinite, i.e., when the independence hypothesis is not valid since angular-momentum distributions in the two systems are not comparable. Finally, we wish to present considerations as to how the reaction effects due to a finite moment of inertia will change with mass region of the compound nucleus.

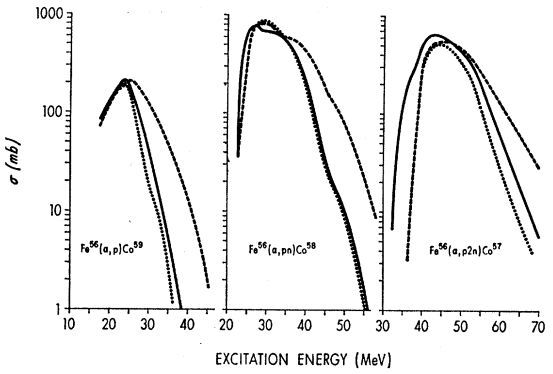

FIG. 3. Calculated excitation functions for reactions of Fe^{56}. The solid curves result from calculations in which an infinite moment of inertia was assumed. The dashed and dotted curves are for calculations in which a rigid-body moment of inertia was assumed; the dashed curves represent integrations using as upper limits the dashed curves of Fig. 1, as given by Eqs. (12). The dotted curves represent an upper integration limit of the binding energy of the least tightly bound nucleon, as given by Eq. (11). The dashed and dotted curves are coincident on the low-energy edges of the excitation functions.

A. Reactions in Fe^{56} Induced with $_2He^4$ Ions

The excitation functions selected for comparisons are those corresponding to reactions in which a proton and one to four neutrons are emitted. These reactions, rather than the (α,xn) reactions, were selected because the shell-structure influence on level densities is considerably less evident in the cobalt-product cross sections than in the nickel products.[29] Without this additional complication, we are able to compare experimental and calculated values directly, with no normalization or adjustment of level-density parameters for shell-structure effects (the effects are present, but do not alter cross sections to the point that comparisons with these calculations are difficult).

Calculated excitation functions for the $Fe^{56}(\alpha,pxn)$ reactions where $x=0$–4 are shown in Figs. 3 and 4;

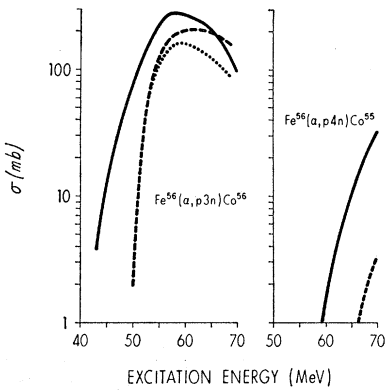

FIG. 4. The curves of this figure have the same significance as those of the preceding figure.

the three sets of excitation functions correspond to calculations for which $R=\infty$, and for which $R=1$ with differing assumptions concerning γ-ray competition [i.e., Eqs. (11) and (12)]. The latter two sets of excitation functions are identical in the region between reaction thresholds to nearly the excitation-function peaks. This is, of course, a consequence of the fact that the $\sigma(Z,A,E,J)$ populations contributing to the products in this region lie predominantly below the thermodynamic binding energy for nucleon emission, as for example in the contour for Ni^{57} in Fig. 1. Note that the integration limits of Eqs. (11) and (12) are applied only in the last stage of the cascade, with the program automatically imposing the limits of Eq. (12) prior to this point, so that both sets of excitation functions show a displacement to higher threshold energy. This results from the removal of available cross section by formation of the high-energy tails of the excitation functions corresponding to the emission of one fewer nucleons, and in this respect a γ-ray cascade prior to reaching the respective products is reflected in both sets of excitation functions. Without this complication in using Eq. (11), the calculated excitation function with $R=1$ would be nearly identical with the $R=\infty$ value in the threshold region as well as at higher energies. As the excitation energy increases, the population in the region between the two limits of integration given by Eqs. (11) and (12) becomes significant, and when it is assumed that this population decays by gamma-ray cascade there results the so-called high-energy tail of the excitation functions, a phenomenon which has been frequently observed, in some cases in predominantly compound-nucleus reactions,[30,31] and in others due to direct-interaction processes.[31]

Comparing calculated excitation functions for which $R=\infty$ with those for which $R=1.0$, we find an increasing displacement of the threshold side of the excitation functions to higher energy (for the $R=1.0$ calculations) as the excitation energy and angular momentum of the compound nuclei increase. This displacement in the (α,pxn) reactions is due to the γ-ray cascade in the $(\alpha, p(x-1)n)$ reactions removing available cross section in forming the increased high-energy tails. The actual thresholds for calculations with both values of R must of course be the same, since there will always be some low-I compound nuclei which need not contribute significantly to the gamma-ray enhancement discussed in Sec. II E. Since the very low cross sections near thresholds are not usually measured experimentally, the apparent displacements predicted in these calculations should be observed. For the limits of integration given by Eqs. (12), with $R=1.0$, the excitation functions peak at higher excitations, and show a much less abrupt decrease with energy past their maxima (i.e., more of a high-energy tail) than do the curves for $R=\infty$. When integrations of the $R=1.0$ populations are performed with the assumption of no γ-ray competition above the minimum nucleon binding energy, there is considerably less difference between the Weisskopf-Ewing and finite-moment-of-inertia calculations. It is worth noting also that there are no large differences in peak cross section between the calculations assuming finite and infinite moments of inertia, and those differences which are observed may be approximately reproduced by a simplified calculation using the s-wave approximation.[32–34] The s-wave approximation assumes that the initial compound-nucleus spin distribution remains constant throughout the emission cascade; this means that the s-wave approximation will actually overestimate the effects predicted by calculations with $R=1.0$, as may be seen by comparing the most probable J in Figs. 1 and 2. Thus, there is no great difference in particle-emission probabilities in these reactions due to an enhancement resulting from strong antiparallel alignment of $\mathbf{I}+\mathbf{l}$; indirect experimental evidence has been presented to substantiate this observation.[35] The differences which are reflected between the different calculations represented in Figs. 3 and 4 result, therefore, primarily from the effect of rotational cooling due to angular momentum, and due to the assumed enhancement of γ-ray cascades due to the spin-forbidden region for particle emission. The latter is the more significant factor in the $A=60$ region, as Figs. 3 and 4 indicate.

Calculations for which $R=\infty$, and for which $R=1$ integrated with the limits of Eqs. (12) are compared with the experimentally measured excitation functions of Ewart *et al.*[15] in Figs. 5 and 6. Where two experimental cross sections were reported at excitations within 1 MeV, the average cross section is plotted at the average excitation. Experimental points are presented only up to those energies for which recoil ranges showed predominantly full momentum transfer reactions.[15] The three lowest cross sections shown for Co^{55} and Co^{66} have been reduced (by approximately 2.5 mb for Co^{56} and 1 mb for Co^{55}) from the values reported to correct for the reaction contributions from the 0.3% Fe^{54} in the targets. Published cross sections for the $Fe^{54}(\alpha,pn)Co^{56}$ and $Fe^{54}(\alpha,p2n)Co^{55}$ reactions were used for this purpose.[36] Since the corrections were comparable in magnitude to the experimental cross sections, the estimated limits of error for these adjusted points have been correspondingly increased.

In the case of the $Fe^{56}(\alpha,pn)Co^{58}$ excitation function, the calculation with $R=1$ and γ-ray emission is in markedly better agreement with the experimental values than the curve for which $R=\infty$. The peaking of both calculated excitation functions around 30 MeV

[30] M. Kaplan and A. Ewart, Phys. Rev. **148**, 1153 (1966).
[31] M. Blann and A. Ewart, Phys. Rev. **134**, B783 (1964).
[32] M. Blann and G. Merkel, Phys. Rev. **137**, B367 (1965).
[33] R. A. Esterlund and B. D. Pate, Nucl. Phys. **69**, 401 (1965).
[34] A. Ewart, thesis, University of Rochester, 1964 (unpublished); available through University Microfilms.
[35] A. Ewart and M. Blann, Nucl. Phys. **72**, 577 (1965).
[36] F. S. Houck and J. M. Miller, Phys. Rev. **123**, 231 (1961).

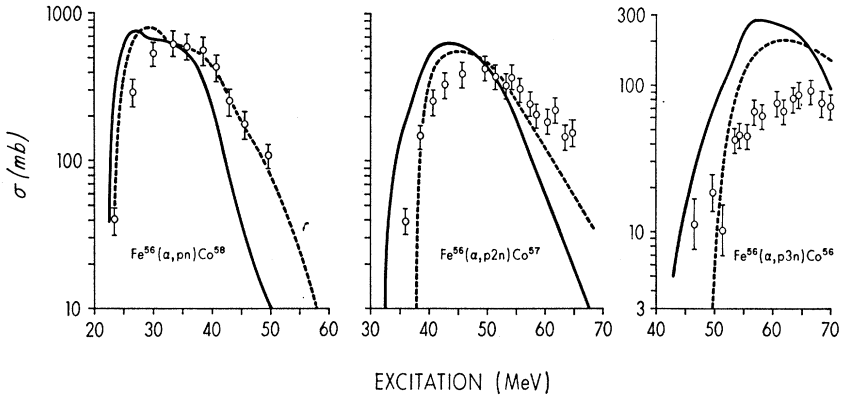

FIG. 5. Calculated and experimental excitation functions for helium-ion–induced reactions of Fe^{56}. Experimental values are represented by open circles with error bars (values are taken from Ref. 15). The solid and dashed curves are identical to those of Figs. 3 and 4.

results from proton emission of 1–3-MeV kinetic energy, the so-called trapped protons due to population in the region where proton binding energies are less than neutron binding energies.[37] The lack of agreement between calculated and experimental excitation functions in this region is indirect evidence that these low-energy protons are not emitted predominantly, but rather that γ rays largely depopulate this region where protons may be emitted only at energies substantially below the Coulomb barrier. More direct evidence that the trapped protons are not emitted from a significant fraction of the total population in the region between proton and neutron binding energies comes from a comparison of the calculated and experimental Fe^{56}-(He^3,p) spectra; many more low-energy protons are calculated then are measured, as may be seen in Fig. 7. The experimental spectrum of Fig. 7 is from the work of Hazan and Merkel.[38]

The calculated (α,$p2n$) excitation function for $R=1.0$ of Fig. 5 is in better agreement with the experimental result than the values from the calculation for which $R=\infty$. The experimental excitation function peaks at a higher energy, and has larger cross sections beyond the peak than the calculated excitation functions. This could be attributed to an underestimate of the point at which γ-ray competition with particle emission becomes significant, an error in the assumed energies below which a given spin may not be populated (which parametrically might be indicated as a decrease in R below 1), or to a more basic cause such as a lifetime too short to permit sufficient statistical sampling in the decay. We have no way at present of deciding which, if any, of these explanations is correct. The experimental (α,$p3n$) and (α,$p4n$) excitation functions are compared with the calculated values in Figs. 5 and 6; little can be said about these comparisons aside from noting the desirability of measurements at higher energies, plus remeasurement of the threshold regions of these reactions to greater accuracy.

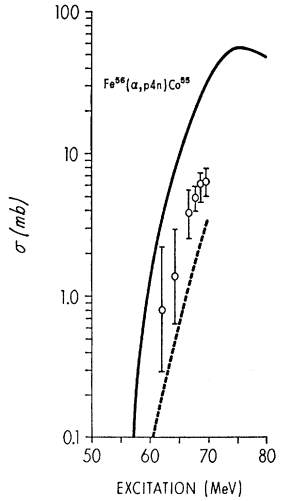

FIG. 6. The points and curves of this figure have the same significance as those of the preceding figure.

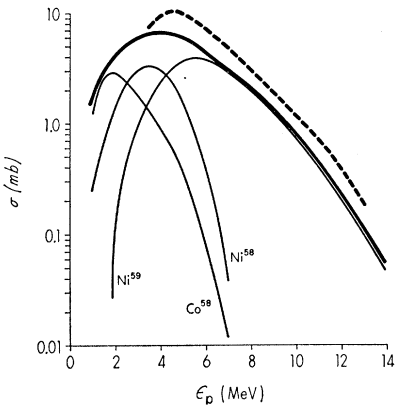

FIG. 7. Calculated and experimental proton spectra resulting from the 10-MeV He^3 bombardment of Fe^{56}. The dashed curve is the experimentally observed spectrum as reported in Ref. 38. The three thin solid curves represent the calculated proton spectra from the Ni^{59} compound nucleus and from the Ni^{58} and Co^{58} daughters. The heavy solid curve is the sum of the calculated spectra from $Ni^{59,58}$ and Co^{58}, showing more low-energy protons than are observed experimentally.

[37] D. Bodansky, R. K. Cole, W. G. Cross, C. R. Gruhn, and I. Halpern, Phys. Rev. **126**, 1082 (1962).
[38] J. P. Hazan and G. Merkel, Phys. Rev. **139**, B835 (1965).

B. Deviations from the Independence Hypothesis due to Angular Momentum

Experiments have been performed in which a given excited nuclear species has been produced with more than one target-projectile combination.[10–12] At a given excitation, the different combinations generally will produce different angular-momentum distributions; comparison of the decay properties of these systems should presumably show the effects of the angular-momentum differences. We have computed the decay of Ni^{60} compound nuclei formed with C^{12} ion bombardment of Ti^{48}($R=1.0$) to compare with the $Fe^{56}(\alpha,pxn)$ reactions previously considered. The excitation functions to be compared were integrated with the limits given by Eqs. (12). Obviously there would be no differences due to angular-momentum effects for calculations in which $R=\infty$.

In comparing calculated or experimental excitation functions resulting from bombardment with different projectiles, it is essential that some sort of normalization be used, such as division of each reaction product cross section by the compound-nucleus cross section leading to that product (or alternatively by comparing ratios of yields of different products in a single system).[36] The importance of this is emphasized in Fig. 8, where the calculated $Ti^{48}(C^{12},pn)Co^{58}$ and $Fe^{56}(\alpha,pn)Co^{58}$ excitation functions are shown. Both sets of calculated values of Fig. 8 were calculated with $R=\infty$; the shift to higher excitation of the C^{12} ion-induced reaction therefore reflects no angular-momentum effect, but rather the Coulomb barrier.

The average angular momentum of the two systems ($Ti^{48}+C^{12}$ and $Fe^{56}+\alpha$) as a function of excitation and bombarding energies is compared in Fig. 9. Because of a higher Coulomb barrier, the $C^{12}+Ti^{48}$ system has the lower angular momentum below approximately 59 MeV of excitation. Excitation functions calculated for the production of Co^{58}, Co^{57}, and Co^{56} in the two systems are compared in Figs. 10–12. In all three cases the system with higher angular momentum is shifted to higher energy with respect to the lower-spin system. The shift amounts to a maximum of 2.5 MeV for the high-energy side of the Co^{58} excitation function, ~1 MeV for the high-energy side of the Co^{57} excitation function, and ~2.5 MeV on the low-energy side of the Co^{56} excitation function. The Co^{56} high-energy tails should cross at an energy in excess of 70 MeV. The predicted differences are large enough to be observed experimentally. Difficulties encountered experimentally are due to uncertainties in the heavy-ion range-energy relationship when these experiments are done by stacked-foil techniques, in addition to the uncertainty in the initial beam energy. Use of some of the newer electrostatic accelerators having easily varied energy heavy-ion beams should improve this situation. A further difficulty in analyzing this type of experiment

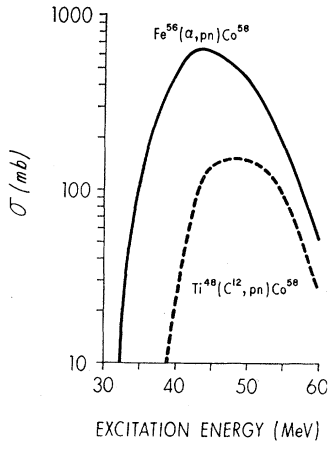

FIG. 8. Calculated excitation functions for helium-ion– and C^{12}-ion–induced production of Co^{58}. The moment of inertia was assumed to be infinite in these calculations, so that the apparent shift to higher energy of the $Ti^{48}(C^{12},pn)$-Co^{58} reaction reflects only the difference in Coulomb barriers.

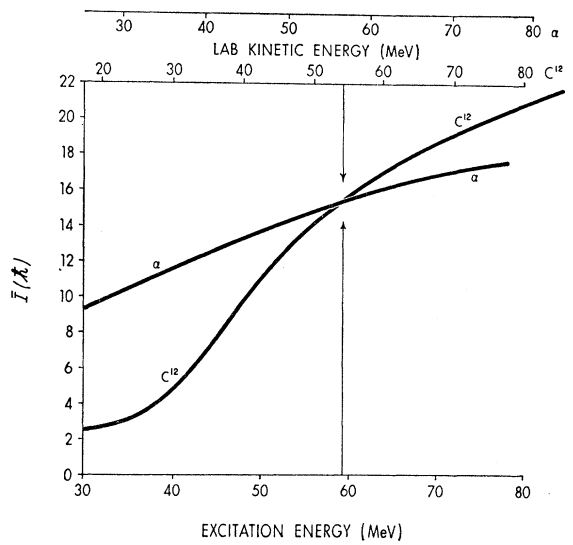

FIG. 9. Comparison of average angular momentum versus energy for Ni^{60} compound nuclei formed by helium-ion bombardment of Fe^{56} and C^{12}-ion bombardment of Ti^{48}, as calculated with the nuclear optical model. The arrows serve to locate the crossover point at approximately 59 MeV of excitation.

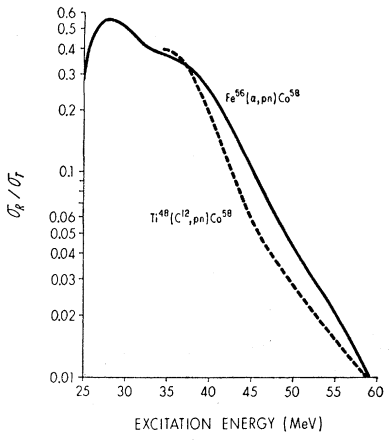

FIG. 10. Comparison of calculated excitation functions for the $Fe^{56}(\alpha,pn)$ and $Ti^{48}(C^{12},pn)$ reactions, assuming a rigid-body moment of inertia and the limits of integration given by Eqs. (12). The ordinate is the ratio of the calculated cross section for the reaction product to the total nonelastic cross section predicted by the optical model.

comes from uncertainty in the values of optical-model parameters to use in calculating total nonelastic cross sections for heavy ions. For these reasons this type of experiment might better be performed with He^3 and He^4 ions where both range-energy and optical-model parameters are better known than for heavy ions, and where the large difference in Q values for He^3- and He^4-induced reactions lead to quite significant differences in angular-momentum distributions at a given excitation energy. The difference in peak yields in the excitation functions of Fig. 11 is consistent with the difference in high-energy tails due to γ-ray emission in the excitation functions of Fig. 10.

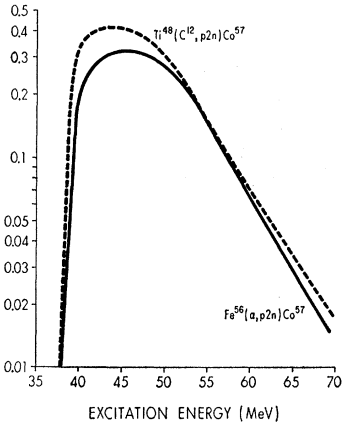

FIG. 11. This figure is similar to the preceding figure, but is for the production of Co^{57}.

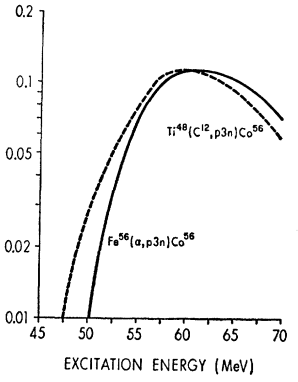

FIG. 12. This figure is similar to Fig. 10, but is for the production of Co^{56}.

C. Variation of Angular Momentum Effects with Mass Number

The manner in which the angular-momentum effects discussed in this section vary with mass number is a worthwhile point for speculation. If the assumption given by Eq. (6) for the spin-cutoff region is assumed for nuclei of mass 24, mass 60, and mass 210, the cutoff curves are given by the solid lines in Fig. 13. Assuming that the compound nuclei are formed with helium ions on neon, iron, and lead targets,[26] the center-of-mass energies versus the most probable spin for the three systems are shown in Fig. 13 as dashed or dotted curves

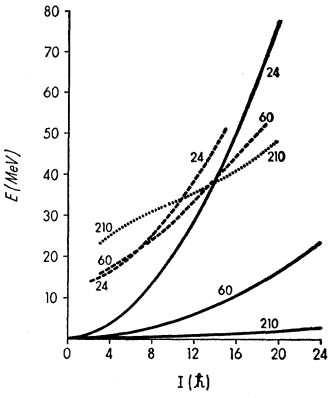

FIG. 13. The solid curves represent the locus of points below which energy the level density is zero for spin I, where the level density given by Eq. (5) has been used with a rigid-body moment of inertia. The curves are for nuclei of mass numbers 24, 60, and 210. The dashed curves and dotted curve represent the loci of most probable angular momentum versus helium-ion kinetic energy for production of nuclei of these masses, based on the optical-model results of Ref. 26.

[the reaction (capture, γ) Q values are not included in the energies shown]. With the assumption that rotational energy ends up in the γ-ray cascade, the energy available for particle emission for each mass number is given by the difference between the excitation-energy curves and the cutoff curve of Fig. 13; i.e., the displacement between the corresponding solid and dashed or dotted curves, if, for simplicity, in a purely qualitative argument, the most probable spin is used to represent the entire spin distribution. These differences are shown somewhat more clearly in Fig. 14 as the energy available for particle emission versus incident helium-ion energy. The dashed 45° line represents the situation one would encounter if R were infinite; the solid curves show that angular-momentum effects with respect to γ-ray–particle-emission competition should be of much less importance in very heavy nuclei than for the $A=60$ systems previously considered in this section, and that these effects should be very much enhanced in a lighter system, such as the $_{10}Ne^{20}+\alpha$ system shown. If the values of Fig. 14 were literally taken to be valid, one would predict a decrease in avilable energy with increasing incident energy for a mass-20 target; one would not expect to observe this phenomenon experimentally,

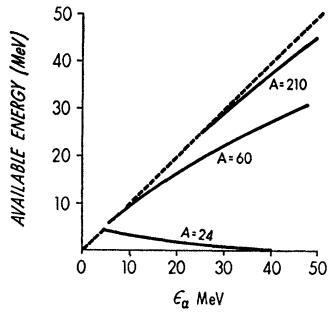

FIG. 14. Energy available for nucleon emission versus incident helium-ion energy (center of mass) for formation of nuclei of mass 24, mass 60, and mass 210. The solid curves are the differences between the corresponding dashed or dotted and solid curves of the preceding figure. The dashed line at 45° represents the situation of all incident energy being available for particle emission; as, for example, if the nuclear moment of inertia were infinite.

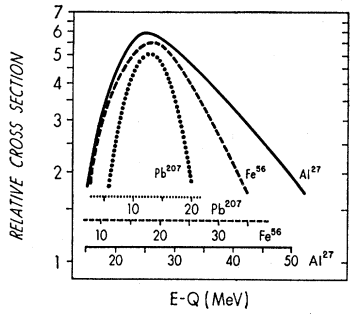

FIG. 15. Comparison of $Pb^{207}(\alpha,3n)Po^{208}$, $Fe^{56}(\alpha,p2n)Co^{57}$, and $Al^{27}(B^{10},p2n)Cl^{24m}$ excitation functions (Refs. 15, 39, 40). The ordinate is in relative units. Excitation function axes have been shifted so as to approximately bring the maximum yields in line vertically. The excitation functions and excitation energies are identified by target symbols. The excitation energies shown represent the compound-nucleus excitations reduced by the appropriate emitted nucleon binding energies, or the energy available for nucleon kinetic energy and gamma-ray emission.

since the highest impact parameters would probably not form compound nuclei in such systems, as is implied by Eq. (5). There are of course too many uncertainties in the crude γ-ray–particle-emission competition assumptions to draw any more than qualitative conclusions from Fig. 14; with decreasing mass number one expects an increase in the high-energy tails, widths, and displacement to higher energies of experimental excitation functions with respect to calculated values for which $R=\infty$, or with respect to experimental values for systems of lower angular momentum, resulting physically from increased γ-ray emission at the lower mass values. A comparison between $Pb^{207}(\alpha,3n)Po^{208}$, $Fe^{56}(\alpha,p2n)Co^{57}$, and $Al^{27}(B^{10},p2n)Cl^{34m}$ excitation functions[15,39,40] is shown in Fig. 15; the qualitative features predicted are in fact present, although direct quantitative comparison of these excitation functions would require a more detailed consideration of the broadening due to differences in nuclear temperature of the three systems, of the relative spin distributions of the boron- and helium-ion–induced reactions, and differences due to a possible increased importance of $\mathbf{I}+\mathbf{l}$ alignment in the $Ne^{20}+\alpha$ system. To the extent that comparisons with calculated excitation functions ($R=\infty$) take account of temperature differences, the conclusions above with respect to increased high-energy tails with decreasing mass number (implying increased γ-ray yields) are supported.[35,40,41]

[39] W. John, Phys. Rev. **103**, 704 (1956); as tabulated in E. K. Hyde, I. Perlman, and G. T. Seaborg, *The Nuclear Properties of the Heavy Elements* (Prentice-Hall, Inc., Englewood Cliffs, New Jersey, 1964), Vol. I, p. 324.

[40] I. M. Landenbauer-Bellis, R. I. Morse, and I. L. Preiss, Nucl. Phys. **88**, 21 (1966).

[41] J. D. Jackson, Can. J. Phys. **34**, 767 (1956).

IV. CONCLUSIONS

Calculated excitation functions for which a rigid-body moment of inertia is assumed, with strong γ-ray versus nucleon emission toward the end of the particle-emission cascade, are in better agreement with experimental values for the $Fe^{56}(\alpha,pn)$ and $(\alpha,p2n)$ reactions than either the same calculation with no γ-ray–particle competition, or a Weiskopf-Ewing calculation, i.e., infinite moment of inertia. There is no great change in peak yields for any of the three calculated sets of excitation functions for the $Fe^{56}(\alpha,pxn)$ reactions, indicating that the rotational cooling effect of angular momentum, with subsequent γ-ray cascade, is more important by far than any effects of strong antiparallel alignment of $\mathbf{I}+\mathbf{l}$ which would tend to enhance higher l waves and therefore higher kinetic energies for emitted particles, and which would enhance emission of neutrons over protons for comparable kinetic energies. For these reasons, the s-wave approximation[32–34] is a very good one for calculations of this type, although it must give an overcorrection with respect to the calculation in which sums are taken over $\mathbf{I}+\mathbf{l}$, as may be seen by comparing the most probable J values toward the end of the particle-emission cascades for $R=1$ and $R=\infty$ (Figs. 1 and 2; the s-wave approximation will have a most probable spin very close to that of the $R=\infty$ value throughout the cascade).

Differences in decay of nuclei produced (in the region $A\sim60$ and below) by α and heavy-ion bombardment should be experimentally observable in excitation-function measurements as long as the enegy of the incident heavy ion is known with sufficient (±0.5 MeV) accuracy. Lack of knowledge concerning reactions with heavy ions (e.g., capture cross sections, optical-model parameters) may make it more desirable to study such reactions with He^3 and He^4 projectiles rather than with heavy ions. Within the simple considerations and arbitrary approximations concerning γ-ray–particle-emission competition of this work, one would expect relatively small effects and low γ-ray yields in heavy elements, with very substantial effects in the lighter elements. This is consistent with the available experimental measurements, as is illustrated by the examples of Fig. 15.

ACKNOWLEDGMENTS

The help and hospitality of Dr. H. Mullish and Dr. M. Goldstein of the New York University–U. S. Atomic Energy Commission computing center is gratefully acknowledged. The author is grateful to L. Schwartz and to J. Cooper for preparation of the plates of this work.